Hindawi
International Journal of Optics
Volume 2021, Article ID 6621939, 8 pages
https://doi.org/10.1155/2021/6621939

Research Article

Multiposition Rotation Interference Absolute Measurement Method for High-Precision Optical Component Surfaces

Xueliang Zhu,[1] **Fengming Nie**,[2] **Bingcai Liu**,[1] **Ruikun Liu**,[1] **and Ailing Tian**[1]

[1]*School of Optoelectronic Engineering, Xi'an Technological University, Xi'an, China*
[2]*Advanced Manufacturing Institute, Inner Mongolia Institute of Metal Materials, Ningbo, China*

Correspondence should be addressed to Xueliang Zhu; zhuxueliang@xatu.edu.cn

Received 7 November 2020; Accepted 2 September 2021; Published 15 September 2021

Academic Editor: Adrian Podoleanu

Modern optical engineering requires increasingly sophisticated interferometry methods capable of conducting subnanometer scale measurements of the large aperture, high-precision optical component surfaces. However, the accuracy of interferometry measurement is limited to the accuracy with which the surface of the reference mirror employed in the interferometer system is known, and the influence of gravity-induced deformation cannot be ignored. This is addressed in the present work by proposing a three-flat testing method based on multiposition rotation interference absolute surface measurement technology that combines the basic theory of N-position rotation with the separability of surface wavefront functions into sums of even and odd functions. These functions provide the rotational symmetric components of the wavefront, which then enables the absolute surface to be reconstructed based on the N-position rotation measurements. In addition, we propose a mechanical clamping combined with computational method to compensate for the gravity-induced deformations of the flats in the multiposition rotation absolute measurements. The high precision of the proposed absolute surface measurement method is demonstrated via simulations. The results of laboratory experiments indicate that the combination compensation method provides the high-precision surface reconstruction outcomes. The present work provides an important contribution for supporting the interferometry measurement of large aperture, high-precision optical component surfaces.

1. Introduction

The development of optical engineering technology has led to systems with increasing complexity, and the optical components are subject to increasingly stringent precision requirements. For example, the surface accuracy of large-scale astronomical telescopes and lithographic lenses has reached the subnanometer scale [1]. This has generated the need for increasingly sophisticated measurement methods, such as wavelength-tuned phase-shift interferometry, that are capable of measuring the subnanometer scale surface accuracy of optical components. However, the surface accuracy of optical components is generally determined as the measured difference between the component surface and a flat reference mirror employed in the interferometer system. Therefore, the accuracy of interferometry measurements is limited by the surface accuracy of the reference mirror, and the impact of reference mirror surface errors on the measurement results is not negligible when the surface accuracy of the reference mirror resides at a comparable level to that of the optical component [2, 3]. Accordingly, the influence of gravity-induced deformation of the reference mirror cannot be ignored in subnanometer scale measurements. Moreover, the increasing aperture sizes of optical components require larger aperture sizes for the interferometer as well, and this increases the extent to which the reference mirrors are subject to gravity-induced deformation.

The primary method employed for determining the effects of reference mirror surface irregularities on the interferometry results obtained for optical components adopts absolute measurement technology to directly measure the surface errors of the reference mirror, which can then be applied to eliminate the influence of these errors on the measurement results [4, 5]. Schulz and Schwider [6] first

proposed the three-flat test method in 1976, which avoids the use of a reference flat by comparing the Fizeau interferometry measurements obtained over four or more measurements for all possible two-flat permutations derived from a set of three flats. Subsequently, Fritz [7] proposed a programmable three-flat test method that represented the obtained interferogram mathematically by fitting them to rotational invariant Zernike polynomials, which were then decomposed into orthogonal basis functions, and the absolute optical surface was reconstructed mathematically by fitting lines to the basis functions using the least squares method. The approach was demonstrated to obtain a closed-form solution if one of the measurements conducted included the azimuthal rotation of one of the flats by some angle. This approach was formalized by Evans and Kestner [8], who proposed the basic N-position rotation theory, which was further developed by Küchel [9] and Lin et al. [10]. In this theory, the measured wavefront is decomposed into a rotationally symmetrical component and a rotationally nonsymmetrical component, and the nonrotational symmetrical component is eliminated by azimuthal rotation through N positions to obtain the absolute optical surface information. Shi et al. [11] applied simulations and experimental analyses to compare the absolute surface reconstruction obtained using the N-position rotation absolute measurement method and an oblique incidence absolute measurement method with three different surface reconstruction algorithms. However, questions remain regarding the optimal number of azimuthal rotations N that should be employed in the method. While a greater number of rotations increase the accuracy of the approach, it also greatly increases the computational burden. Moreover, the calculation of the rotationally symmetric components is subject to error, which negatively detracts from the reconstruction accuracy. In a parallel development to N-position rotation methods, Ai and Wyant [12] proposed a surface reconstruction method similarly based on the three-flat test method with mathematically represented interferogram. However, the method employed the separability of surface wavefront functions into sums of even-odd, odd-even, even-even, and odd-odd functions and obtained these function components by conducting interferometry measurements under eight orientations measuring three flats, where one of the flats in each measurement was rotated by 180°, 90°, and 45° with respect to the stationary flat. The even-odd and odd-even functions were first obtained, from which the even-even function was calculated. Then, the components of the odd-odd function were estimated based on the array of experimental results, and the absolute surface was reconstructed based on all available function components.

Different methods for providing highly accurate surface characterizations of optical components have been developed by directly analyzing the gravity-induced deformations of the components. For example, Wang et al. [13] extended this basic approach by physically compensating for gravity-induced deformation through the direct application of a force to the edge of a frame holding the optical component as a means of inducing a counteracting gravity-induced deformation. Here, the position and magnitude of the force were optimized based on elastic shell theory models of large aperture optical components to get the best deformation compensation effect. In addition, Dewitt et al. [14] developed equations for describing the gravity-induced deformation of optical lenses, and the effects of lens size, material, and mounting method on the deformation were analyzed. These methods could be conceivably employed to compensate for the gravity-induced deformation of large aperture reference mirrors employed in interferometer systems used for measuring the surface accuracy of high-precision optical components.

The present work addresses the limitations of past work by proposing a modified three-flat testing method based on multiposition rotation interference absolute measurement technology, which combines the N-position rotation theory with the separability of functions. The Zernike polynomials fitting algorithm was used usually. However, here, the measured wavefronts are decomposed into even-odd, odd-even, even-even, and odd-odd functions. These functions are then employed to obtain the rotational symmetric components of the wavefronts in conjunction with an N-averaging algorithm. Finally, the absolute surface is reconstructed based on the N-position rotation measurements. In addition, we propose a mechanical clamping method to compensate for the gravity-induced deformations of the three flats in the multiposition rotation absolute measurements when the materials and dimensions of the flats are determined to be known. Different from the listed references, as well as a computational compensation method that is applicable even when the materials and/or dimensions are changed, the results of simulations demonstrate that average root-mean-square (RMS) differences between mathematically generated irregular surfaces and the surfaces reconstructed by the proposed multiposition rotation absolute measurement method are less than 0.003 nm, while the average peak-to-valley (PV) differences are less than 0.01 nm. The results of laboratory experiments indicate that the compensation method provides the high-precision surface reconstruction outcomes.

2. Theoretical Basis of Multiposition Rotation Absolute Measurements

The measurement principle of the N-position rotation method is illustrated in Figure 1, which involves three circular optical flats, A, B, and C, in different Fizeau interferometer configurations. We note that flat A is always on the top and flat B is always on the bottom, while flat C is on both the top (where it is referred to as C_s) and bottom positions. We also note that the flat in the top position always has a $(-x, y)$ orientation, while the flat in the bottom position generally has a (x, y) orientation, but may have $(-x, -y)$ or an orientation (r) that varies in uniform angular displacements $\Delta\theta$; through a complete 360° rotation relative to the top flat, the rotation axis z is perpendicular to the measured surface.

For a wavefront function $W(r, \theta)$ in polar coordinates, the rotationally symmetric component W_r (r, θ) can be expressed as

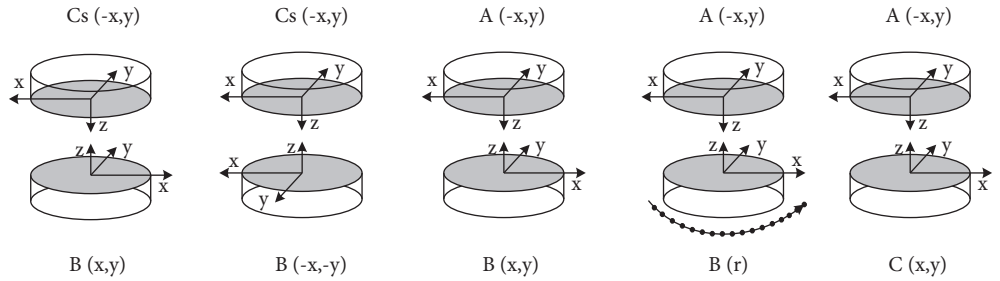

Figure 1: Schematic illustrating the N-position rotation method for reference mirrors A, B, and C in different Fizeau interferometer configurations.

$$W_r(r,\theta) = \frac{1}{2\pi}\int_{\theta=0}^{2\pi} W(r,\theta)\,\mathrm{d}\theta. \tag{1}$$

Here, $W_r(r, \theta)$ is an odd-odd function. Moreover, it is rotationally invariant and is therefore constant with respect to $\Delta\theta$. The integral in equation (1) can be approximated as a sequence of N discrete steps as follows:

$$W_r(r,\theta) = \frac{1}{2\pi}\int_0^{2\pi} W(r,\theta)\,\mathrm{d}\theta = \lim_{N\longrightarrow\infty}\left[\frac{1}{2\pi}\sum_{k=0}^{N-1} W(r,\theta)\Delta\theta_k\right]$$
$$\approx \frac{1}{N}\sum_{k=0}^{N-1} W(r,k\Delta\theta) \approx \frac{1}{N}\sum_{k=0}^{N-1} W(r,\theta-k\Delta\theta). \tag{2}$$

Here, the approximation introduces the uniform angular increment $\Delta\theta = 2\pi/N$. Accordingly, the rotationally symmetric components can be obtained by rotating the wavefront function $W(r, \theta)$ by N equally spaced angular intervals $\Delta\theta$. These wavefront functions can be correlated with interferometry measurements for the three optical flat configurations illustrated in Figure 1 to obtain the following rotationally symmetric components:

$$\begin{cases} W_1 = A(-x,y) + B(x,y), \\ W_2 = A(-x,y) + C(x,y), \\ W_3 = C(-x,y) + B(x,y), \\ W_4 = C(-x,y) + B(-x,-y), \\ W_5 = A(-x,y) + B_{\mathrm{rot}}(x,y). \end{cases} \tag{3}$$

As discussed, $B(r)$ represents the rotation of flat B about flat A through N equally spaced rotations of angular interval $\Delta\theta = 2\pi/N$. Accordingly, W_5 can be expressed as follows:

$$W_5(x,y) = \frac{1}{N}\sum_{k=0}^{N-1}\left\{C(-x,y) + [B(x,y)]^{k\Delta\theta}\right\}$$
$$= C(-x,y) + \frac{1}{N}\sum_{k=0}^{N-1}[B(x,y)]^{k\Delta\theta} \tag{4}$$
$$\approx C(-x,y) + B_r(x,y).$$

Here, $B_r(x, y)$ represents the rotational invariant component of the wavefront function $B(x, y)$ of flat B. Accordingly, the odd-odd function of the flat B can be eliminated from $W_5(x, y)$. Then, $W_5(x, y)$ includes only the odd-odd function of flat C (i.e., $W_{5oo} \approx -C_{oo}$).

Using flip and mutual operations along the x and y axes, together with the odd and even function method, enables the odd-even, even-odd, and odd-odd function terms of the three flats to be measured. In addition, all function terms of flat C can be solved because the $W_5(x, y)$ wavefront contains only the odd-odd function term of flat C. Accordingly, the function term components of flats A and B can be obtained by, respectively, substituting the calculated function components of flat C into the other wavefronts. The absolute surfaces of the three flats are then obtained as follows:

$$\begin{pmatrix} A(x,y) \\ B(x,y) \\ C(x,y) \end{pmatrix} = \frac{1}{240}\begin{pmatrix} 90 & 30 & 30 & -30 & 90 & 30 & 30 & -30 & -45 & -45 & 15 & 15 & -45 & 15 & -45 & 15 & 60 & -60 & -60 & 60 \\ -6 & 86 & 46 & -6 & -54 & -26 & 14 & -54 & 13 & 77 & -23 & -7 & -7 & 77 & -23 & 13 & 60 & -60 & -60 & 60 \\ -54 & -26 & 14 & -54 & -6 & 86 & 46 & -6 & 77 & 13 & -7 & -23 & -23 & 13 & -7 & 77 & 60 & -60 & -60 & 60 \end{pmatrix} \times$$
$$\cdot\begin{bmatrix} W3(x,-y) & W3(-x,-y) & W4(x,y) & W4(-x,y) & W4(x,-y) & W4(-x,-y) & W5(x,y) \\ & & & W5(-x,y) & W5(x,-y) & W5(-x,-y) & \end{bmatrix}^{\mathrm{T}}. \tag{5}$$

3. Simulation of Multiposition Rotation Absolute Measurements

The simulations employed three flats $A(x, y)$, $B(x, y)$, and $C(x, y)$ generated by Zernike polynomials with the coefficients being set to obtain surfaces with substantially different irregularities, but with average deviations from a perfect plane which were nearly equivalent. This yielded average PV errors of 14.39 nm, 15.61 nm, and 13.88 nm for flats A, B, and C, respectively, and average RMS errors of 2.19 nm, 2.86 nm, and 2.57 nm, respectively. The surface topographies are shown in Figure 2. The proposed absolute measurement process was evaluated for the three flats based on the simulated wavefront obtained under the proposed processing.

We first evaluated the effect of the selected value of N on the simulated measurement results for values of N in the range from 3 to 12. According to the described method, the wavefront calculated by equation (4) is flipped along the x and y axes, the required components are calculated, and the absolute surfaces are obtained by equation (5). The RMS differences between the generated surface and the reconstructed surface (i.e., RMS errors) were calculated, and the distributions of the RMS errors obtained for flat A with N values of 3, 6, 9, and 12 are presented in Figures 3(a)–3(d), respectively. We note that the error distributions vary widely for N values of 3 and 6, but are reasonably stable for N values of 9 and 12, indicating that little benefit is gained by employing $N = 12$. The distributions of RMS errors obtained for flats A, B, and C with $N = 9$ are presented in Figures 4(a)–4(c), respectively. In addition, the average RMS errors were all less than 0.001 nm, while the average PV errors were all less than 0.01 nm.

We also evaluated the extent to which the average magnitude of deviations of the generated flats impacted the accuracy of the reconstructed surfaces obtained with $N = 9$. This was evaluated by generating the same characteristic flats A, B, and C shown in Figure 2 using Zernike polynomials with the coefficients being set to obtain surfaces with average deviations, every group flat was nearly in the approximate interval and varied in terms of the average PV errors in the range of 10–200 nm. The reconstructed surfaces were obtained according to the proposed method, and the PV and RMS differences between the initialed and reconstructed surfaces were calculated. The PV value varies between 0.009 nm and 0.011 nm, and the RMS value varies between 0.002 nm and 0.004 nm. These results are presented in Figure 5 with respect to the average deviation of the generated surfaces from the initial plane. The results demonstrate that the magnitude of the average deviation of the generated surfaces from the initial plane has a negligible effect on the accuracy of the surfaces reconstructed using the proposed method, even when the initial plane deviation is as large as 200 nm. Accordingly, the simulation results indicate that the multiposition rotation absolute surface measurement method has better accuracy under different initial surface shape error conditions.

4. Gravity-Induced Deformation Compensation and Experimental Analyses

4.1. Gravity-Induced Deformation Compensation Model. The measured planes are placed horizontally and vertically usually, according to two types of common structures in the field of high-precision interferometry of plane shape. The influence of gravity and clamping deformation in horizontal structures is very obvious. Especially the gravitational effect plays an important role and is evenly distributed and controllable. In opposition, the gravity deformation of vertical structures has little influence and it is also difficult to accurately control the clamping deformation. In addition, it is easier to adapt a horizontal structure to the actual processing state and it is more convenient to transfer and adjust it in the process, so the horizontal structures present some advantages. The goal of gravity-induced deformation compensation is to eliminate the deformation error caused by gravity from the absolute measurement results. The deformation conditions of the top and bottom flats can be analyzed according to Figure 6. As shown in Figure 6(a), flat C exhibits deformation when it is on the top. However, Figure 6(b) indicates that flat C is nearly free of deformation when on the bottom. The asymmetrical deformations associated with these two conditions represent varying optical path length differences that introduce deviations from the ideal wavefront expressions in equation (3). However, if the materials and dimensions of the two flats are equivalent, the mechanical clamping compensation method illustrated in Figure 6(c) can be employed. Here, the flats A and C are supported by equivalent clamping methods, which induce roughly equivalent deformations on their surfaces. Accordingly, this significantly reduces the extent to which the optical path length differences illustrated in Figures 6(a) and 6(b) differ, thereby reducing the influence of the clamping deformation on the measurement results.

When the materials and/or dimensions of the flats differ, the mechanical compensation method will present uncertainty and cannot be applied with reasonable success. Therefore, the standard measurement configuration must be employed with the bottom flats placed directly below on the planar surface as usual and the top flats subject to gravity-induced deformation. However, in the proposed method, only flats A and C_s are placed in the top position. Therefore,

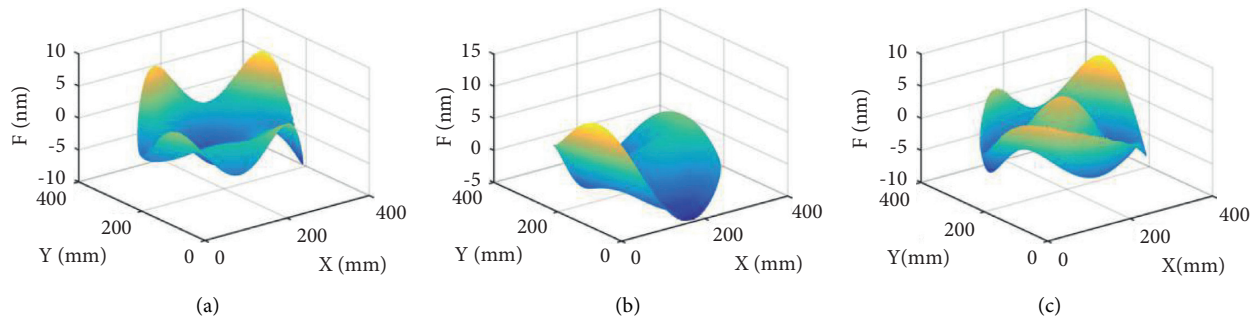

Figure 2: Surfaces of flats generated by Zernike polynomials: (a) flat A, (b) flat B, and (c) flat C. The deviations of all three surfaces from a perfect plane are nearly equivalent.

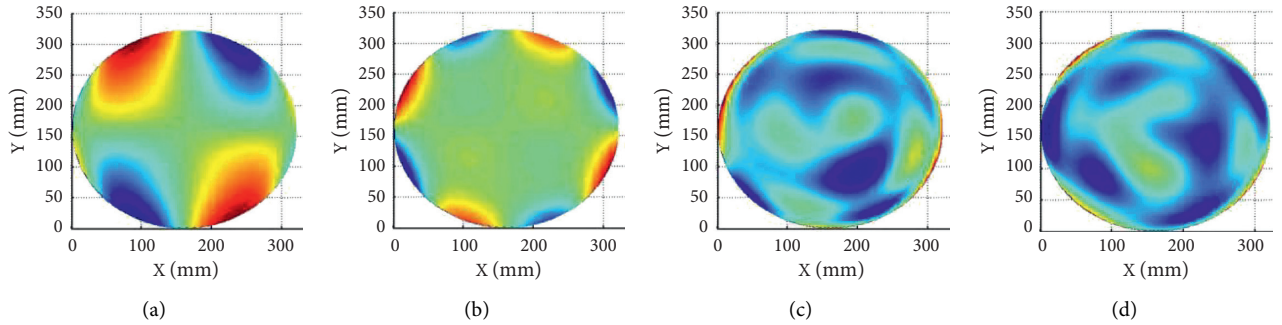

Figure 3: Distributions of root-mean-square (RMS) differences between the generated surface and the reconstructed surface obtained for flat A with different numbers of measurement rotations N: (a) $N = 3$, (b) $N = 6$, (c) $N = 9$, and (d) $N = 12$.

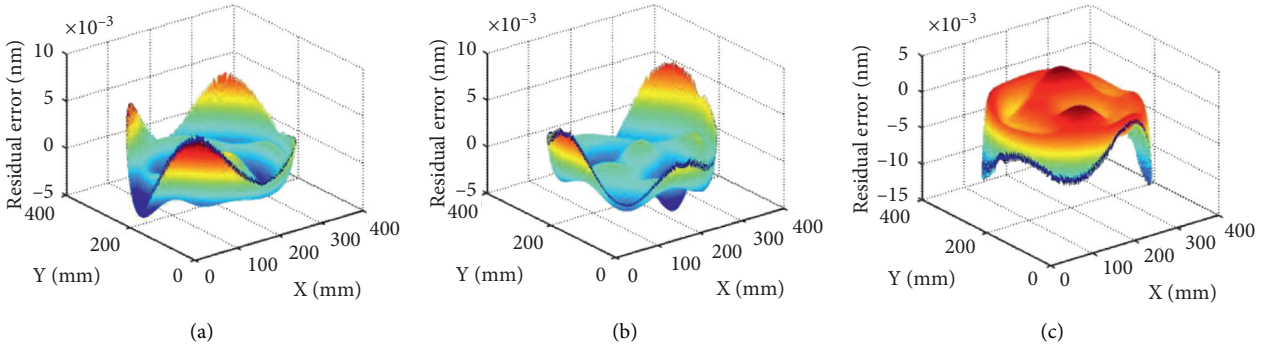

Figure 4: Distributions of root-mean-square (RMS) differences between the generated surfaces and the reconstructed surfaces obtained with $N = 9$: (a) flat A, (b) flat B, and (c) flat C.

only these flats introduce clamping deformation into the measurements. Accordingly, the wavefront expressions in equation (3) can be revised as follows:

$$\begin{cases} W_{s1} = A(-x, y) + w_a(x, y) + B(x, y), \\ W_{s2} = A(-x, y) + w_a(x, y) + C(x, y), \\ W_{s3} = C(-x, y) + w_c(x, y) + B(x, y), \\ W_{s4} = C(-x, y) + w_c(x, y) + B(-x, -y), \\ W_{s5} = A(-x, y) + w_a(x, y) + B_{\text{rot}}(x, y). \end{cases} \tag{6}$$

Here, $w_a(x, y)$ represents the wavefront due to the deformation of flat A and $w_c(x, y)$ represents wavefront due to the deformation of flat C_s. These deformation wavefronts can be calculated for flats with various materials, dimensions, thicknesses, and clamping mechanisms and assembled into a deformation wavefront database. The present work assembled a deformation wavefront database based on deformation calculations using a thin plate model and finite element simulations. Then, the calculated values of $w_a(x, y)$ and $w_c(x, y)$ can be subtracted from the measured wavefront W_{s1}–W_{s5} to obtain reasonable approximations of the ideal wavefront expressions givens in equation (3). Furthermore, the wavefronts W_{s1}–W_{s5}, respectively, represent the new wavefronts obtained from each combination of interference fringes captured during the absolute measurement process, which contain deformation data.

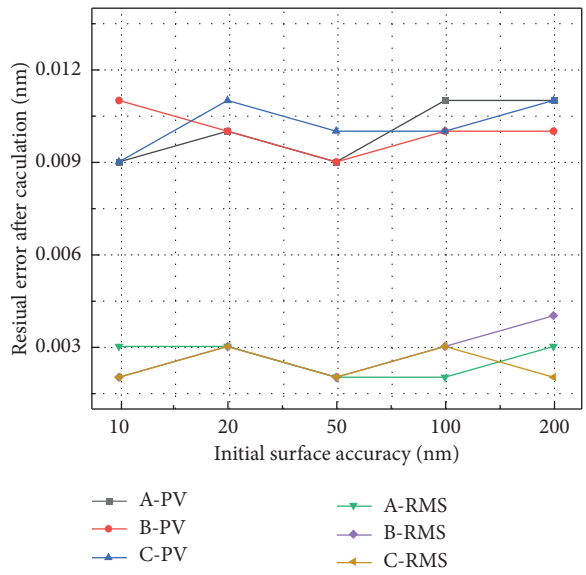

Figure 5: Peak-to-valley (PV) and root-mean-square (RMS) differences between reconstructed surfaces obtained with $N = 9$ and generated surfaces A, B, and C with respect to the average deviation of the generated surfaces from a perfect plane. The deviations of all three surfaces from a perfect plane are nearly equivalent in all cases.

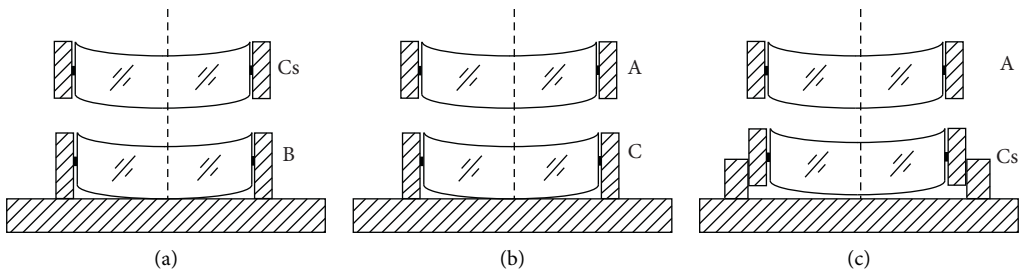

Figure 6: Schematic illustrating various clamping states: (a) standard clamping with flat C_s on the top and flat B in contact with a planar surface, (b) standard clamping with flat A on the top and flat C in contact with a planar surface, and (c) proposed deformation compensation method with flat A clamped on the top and flat C_s similarly clamped below.

The present work therefore provides a mechanical clamping structure combined with a computational method to compensate for the gravity-induced deformations of the three flats in the multiposition rotation absolute measurements when the materials and dimensions are equivalent. Naturally, the computational compensation method is fully applicable as well when the materials and dimensions of the flats are different.

4.2. Results and Analysis of Absolute Surface Measurement Experiments. The surface reconstruction performance of the proposed multiposition rotation absolute measurement method in conjunction with the corresponding deformation compensation was evaluated experimentally using three reference mirrors fabricated with equivalent materials, dimensions, and surfaces having an average PV deviation of about 20 nm by theoretical estimation. In addition, the same clamping mechanism structure was applied to all mirrors during the experiments, where the frames were only glued on their sides to ensure consistent clamping deformations according to Figure 6. The experiments used a vertical Fizeau wavelength-tuned interferometer with a common-path design, an aperture of 300 mm, and a variable frequency laser with a power of 30 mW and a center wavelength of 688 nm. Multiposition rotation absolute measurements were obtained with $N = 10$, and the effect of random errors on the measurement results were reduced by basing each measurement result on an average of ten measurement data.

First, we evaluated the surface reconstruction performance of the proposed computational method to compensate for the gravity-induced deformations of reference mirrors A and C in the multiposition rotation absolute measurements. Accordingly, interferometric wavefront measurements $W_{s1}(x, y)$, $W_{s2}(x, y)$, $W_{s3}(x, y)$, $W_{s4}(x, y)$, and $W_{s5}(x, y)$ were obtained. Substituting the average values into equation (6) and subtracting the calculated values of $w_a(x, y)$ and $w_c(x, y)$ yield the reconstructed surfaces of reference mirrors A, B, and C shown in Figures 7(a)–7(c), respectively. The average PV deviations from a perfect plane obtained for the three mirrors were 15.22 nm, 16.34 nm, and 14.95 nm, respectively.

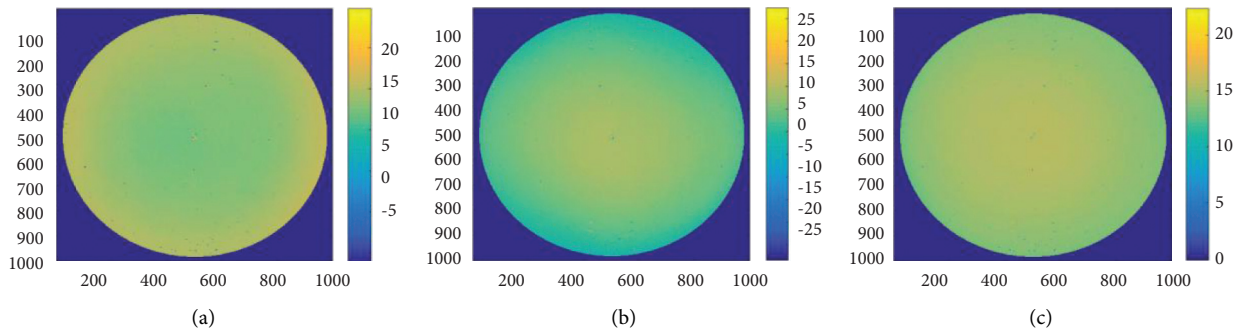

Figure 7: Distributions of peak-to-valley (PV) deviations from a perfect plane obtained experimentally for the reconstructed reference mirror surfaces using the proposed computational method to compensate for the gravity-induced deformations of the three reference mirrors in the multiposition rotation absolute measurements conducted with $N = 10$: (a) upper surface of reference mirror A, (b) upper surface of reference mirror B, and (c) upper surface of reference mirror C.

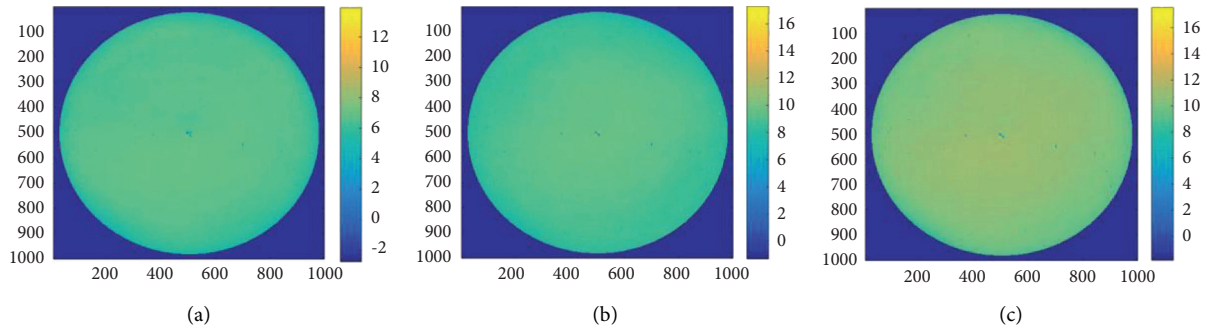

Figure 8: Distributions of peak-to-valley (PV) deviations from a perfect plane obtained experimentally for the reconstructed reference mirror surfaces using the proposed mechanical clamping method to compensate for the gravity-induced deformations of the three reference mirrors in the multiposition rotation absolute measurements conducted with $N = 10$: (a) upper surface of reference mirror A, (b) upper surface of reference mirror B, and (c) upper surface of reference mirror C.

Next, we evaluated the surface reconstruction performance of the proposed mechanical clamping combined with computational method applied to reference mirror C in the multiposition rotation absolute measurements. Accordingly, interferometric wavefront measurements $W_1(x, y)$, $W_2(x, y)$, $W_3(x, y)$, $W_4(x, y)$, and $W_5(x, y)$ were obtained. Substituting the average values into equation (3) yields the reconstructed surfaces of reference mirrors A, B, and C shown in Figures 8(a)–8(c), respectively. The average PV deviations from a perfect plane obtained for the three mirrors were 11.70 nm, 12.41 nm, and 11.25 nm, respectively.

Comparing the results of the compensation methods with the reconstructed surfaces in Figure 4, we note that the maximum PV deviation was 1.7 nm from a perfect plane obtained for mirrors A, B, and C by the mechanical clamping combined with the computational compensation method. The results indicate that the combination compensation method provides the high-precision surface reconstruction outcomes.

5. Conclusion

The present work addressed the limitations of past work by proposing a modified three-flat testing method based on multiposition rotation interference absolute surface measurement technology that combines the basic theory of N-position rotation with the separability of surface wavefront functions into sums of even and odd functions. In addition, we proposed a mechanical clamping combined with computational method to compensate for the gravity-induced deformations of the three flats in the multiposition rotation absolute measurements when the materials and dimensions of the flats are equivalent. The results of simulations demonstrated that the average PV differences between mathematically generated irregular surfaces and the surfaces reconstructed by the proposed multiposition rotation absolute measurement method are less than 0.1 nm. The results of laboratory experiments demonstrated that the deformation compensation method provides sufficiently high-precision surface reconstruction outcomes. Accordingly, we conclude that the present work provides an important contribution to the field of interferometry measurements of large aperture, high-precision optical component surfaces.

Data Availability

The simulation analysis data and experimental measurement data used to support the findings of this study are included within the article.

Conflicts of Interest

The authors declare that they have no conflicts of interest.

Acknowledgments

The authors thank LetPub (http://www.letpub.com) for its linguistic assistance and scientific consultation during the preparation of this manuscript. This research was funded by National Basic Scientific Research (JSZL2018411C001) and Scientific Research Project of Shaanxi Provincial Department of Education (21JY019).

References

[1] S. Jiang, Y. Ding, W. Miao et al., "Recent progress of inertial confinement fusion experiments in China," *Science China Physics, Mechanics & Astronomy*, vol. 39, pp. 1571–1583, 2009.

[2] X. Zhu, H. Zhao, L. Dong et al., "High-precision self-adaptive phase-calibration method for wavelength-tuning interferometry," *Measurement Science and Technology*, vol. 28, no. 3, Article ID 035203, 2017.

[3] R. Liu, "Research on absolute testing technology of standard plane based on multi-flat mutual inspection," Master's Thesis, Xi'an Technological University, Xi'an, China, 2020.

[4] M. Vannoni and G. Molesini, "Absolute planarity with three-flat test: an iterative approach with zernike polynomials," *Optics Express*, vol. 16, no. 1, pp. 340–354, 2008.

[5] X. Zhu, D. Wang, F. Nie, B. Liu, H. Wang, and A. Tian, "Large-aperture real-time compensated collimating wavefront error detection method," *Applied Sciences*, vol. 9, no. 11, p. 2370, 2019.

[6] G. Schulz and J. Schwider, "IV interferometric testing of smooth surfaces," in *Progress in Optics*, E. Wolf, Ed., vol. 13, pp. 93–167, Elsevier, Amsterdam, Netherlands, 1976.

[7] B. S. Fritz, "Absolute calibration of an optical flat," *Optical Engineering*, vol. 23, no. 4, pp. 379–383, 1984.

[8] C. J. Evans and R. N. Kestner, "Test optics error removal," *Applied Optics*, vol. 35, no. 7, pp. 1015–1021, 1996.

[9] M. F. Küchel, "A new approach to solve the three flat problem," *Optik*, vol. 112, no. 9, pp. 381–391, 2001.

[10] W. Lin, Y. He, L. Song, H. Luo, and J. Wang, "Absolute surface metrology by rotational averaging in oblique incidence interferometry," *Applied Optics*, vol. 53, no. 16, pp. 3370–3378, 2014.

[11] M. Shi, L. Shijie, C. Lei, Z. You, and B. Yunbo, "Simulation and experimental study of absolute measurement method for optical surface," *Laser & Optoelectronics Progress*, vol. 55, no. 5, Article ID 051201, 2018.

[12] C. Ai and J. C. Wyant, "Absolute testing of flats by using even and odd functions," *Applied Optics*, vol. 32, no. 25, pp. 4698–4705, 1993.

[13] R. D. Wang, P. Wang, W. Tian, L. P. Wang, Y. X. Sui, and H. J. Yang, "Design and analysis of compensation of large aperture optical element for gravity deformation," *Chinese Optics*, vol. 4, pp. 259–263, 2011.

[14] F. DeWitt IV, G. Nadorff, and M. Naradikian, "Self-weight distortion of lens elements," in *Current Developments in Lens Design and Optical Engineering VII*, P. Z. Mouroulis, W. J. Smith, and R. B. Johnson, Eds., SPIE, Bellingham, WA, USA, Article ID 62880H, 2006.